Mathematical Biosciences and Engineering

MBE, 19(6): 5717–5737.
DOI: 10.3934/mbe.2022267
Received: 04 December 2021
Revised: 18 January 2022
Accepted: 20 March 2022
Published: 02 April 2022

http://www.aimspress.com/journal/MBE

*Research article*

# Investigation of braided stents in curved vessels in terms of "Dogbone" deformation

**Chen Pan[1,2], Xinyun Zeng[2], Yafeng Han[1,*] and Jiping Lu[1]**

[1] School of Mechanical Engineering, Beijing Institute of Technology, Beijing 100081, China
[2] Institute of Engineering Medicine, Beijing Institute of Technology, Beijing 100081, China

* **Correspondence:** Email: hanyafeng@bit.edu.cn; Tel: +8618813078613.

**Abstract:** "Dogbone" deformation that the diameters of two ends are larger than the middle diameter of the stent under the effect of the balloon expanding, is one of the important standards to evaluate the mechanical properties of vascular stents. It is a huge challenge to simulate and evaluate the "Dogbone" behaviors of braided stents in the curved vessels. In this study, the key work was to investigate the "Dogbone" deformations of braided stents in the curved vessels by designing main parameters including strut diameter, braiding angle, and the circumferential number of unit cell. Based on the "Dogbone" stents in the curved vessels, the impact of "Dogbone" on the fatigue properties of braided stents was analyzed under the pulsatile effect of vessels. The influence of "Dogbone" stents on stress distribution of vascular walls was studied. To evaluate the "Dogbone" behaviors of stents in the curved vessels, the calculation method of "Dogbone" was improved by calculating the centerline and the bus bar of the curved vessels. Braided stents with various parameters (strut diameter $t$ = 100, 125 and 152 μm, braiding angle $\alpha$ = 30, 40 and 50°, the circumferential number of unit cell $N$ = 8, 10, and 12) were designed respectively. Numerical simulation method was used to mimic the "Dogbone" deformation after stent expansion. The results showed that strut diameter and braiding angle had more influence on "Dogbone" deformations than the circumferential number of unit cell. "Dogbone" deformation could adversely affect fatigue performance and vascular walls.

**Keywords:** braided stents; strut diameter; braiding angle; the circumferential number of unit cell; "Dogbone" deformation; fatigue performance; stress distribution of vascular walls

## 1. Introduction

The stent is a sophisticated medical device, which is used to treat atherosclerosis and other blocked cardiovascular diseases. The braided stent is one of the earliest vascular stents used in clinical applications to treat aneurysms and guide blood flow [1]. The braided stent can withstand large deformation because each strut has the capacity of sliding or rotating relative to each other [2]. The braiding angle that is the angle between struts (as shown in Figure 1(a) normal expansion of stent) affecting the mechanical behavior of braided stent is still a recent research issue. Mckenna and Vaughan [2,3] investigated the mechanical properties of the bare-metal and covered braided stents by changing the various angles of wires. They concluded that braiding angle was a key impact factor on the deformations of bare-metal and covered braided stents. Similarly, Ueng et al. [4] also considered that braiding angle influenced the braiding structure property. Apart from the braiding angle, Zhang et al. [5] discussed the influence of the braiding strut number and strut diameter on the mechanical characterizations, they found the braiding angle and the diameter of strut were two key design factors for braided stents because of affecting radial stiffness and longitudinal flexibility. For bioresorbable braided stents, Zhao et al. [6] and Sun et al. [7] researched the mechanical stability during degradation of the poly (p-dioxanone) (PPDO) braided stents. In terms of structure, Shanahan et al. [8] designed looped ends and open ends braided stents and used finite element analysis to evaluate the performance of the two braided stents. But these kinds of literature on braided stents are based on straight vessels and do not discuss the mechanics of stents in curved vessels.

It is an enormous challenge to evaluate the mechanics of stents in the curved vessels. For one thing, due to the influence of structure and material properties, the axial "straightening" of the stent will occur in the process of expanding, and there will be geometric nonlinear contact and deformation between stent and the curved vessels, resulting in the non-convergence of finite element numerical analysis. For another, it is difficult to accurately deliver and release stents in the curved vessels in vitro experiments. However, scholars tried to study the mechanical performance after stents expanding in the curved vessels [9−11]. Wu et al. [12] designed two stents for studying the In-stent restenosis (ISR) in a curved vessel. However, because of the small degree of vessel curvature, stents had a strong straightening effect on the vessels. Kasiri and Kelly [13] put forward to deployment of multiple shorter stents instead of a longer stent in a curved vessel. They had the conclusion that multiple shorter stents could provide higher flexibility, more conformity, and lower recoil in comparison with a long stent. Han and Lu [14] proposed the non-uniform Poisson's ratio structural stent, the result showed the stent with a nonuniform Poisson's ratio could perfectly fit into the curved artery after expansion.

There are some important requests for a stent having good material properties and mechanical behaviors in clinical medicine. According to Food and Drug Administration (FDA), there are some items to evaluate the performance of stents including flexibility, radial stiffness, foreshortening, longitudinal recoil, radial recoil, "Dogbone", and fatigue durability. Therefore, the mechanical behaviors of stents are worth being discussed in research kinds of literature [15−21]. Prithipaul et al. [22] evaluated the mechanical behaviors of five different structural stents, including the foreshortening, radial stiffness, and elastic recoil. They pointed out that it was difficult for a stent to have multiple good mechanical properties. Maleckis et al. [23] compared and assessed the performance of twelve stents under bending and torsion deformations quantitatively and qualitatively in terms of force-strain behavior, stiffness, and geometrical shape. But they found

none of the stents demonstrated superior mechanical behaviors under all deformation modes. Among evaluation items, "Dogbone" deformation is one of the most intractable problems, which causes serious impacts on fatigue of stent and blocked vessel. "Dogbone" deformation of stent often occurs utilizing balloon-expanding, the expansion of the distal zone is stronger concerning to compared to the central zone [24,25]. In Figure 1, clinical expansion of stent only opens up the vascular vessel, but the "Dogbone" expansion of stent can result in larger deformation of the vessel wall. "Dogbone" is extremely harmful to blood vessels, which triggers larger mechanical stress on the vascular wall and increases the risk of ISR [26]. "Dogbone" is a very complicated deformation during the stent expanding process. There is a small amount of papers about the "Dogbone" deformation of stent in the curved vessels. The curvature degree of blood vessels studied in these literatures is small, for example, a central angle 30° of the vessel designed by Wei et al. [11]. In addition, the stress concentration of "Dogbone" stent and the damage to vascular wall have not been studied and analyzed in detail. Therefore, the "Dogbone" behaviors of braided stents on the curved artery need to be studied.

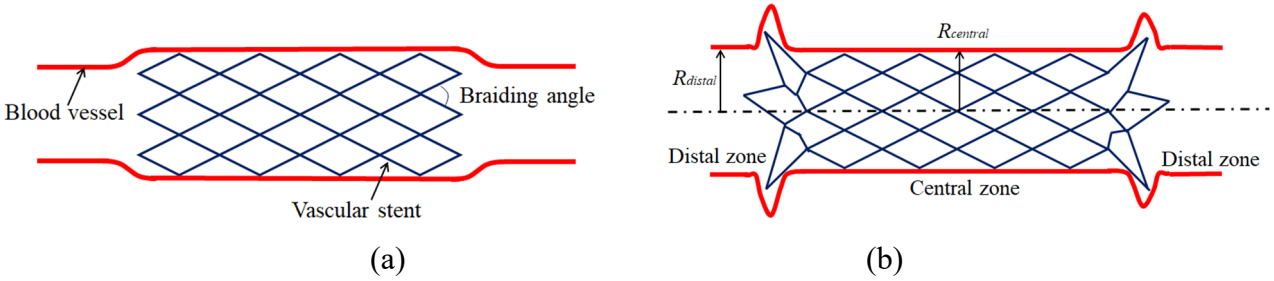


**Figure 1.** Expansion of braided stents: (a) normal expansion; (b) "Dogbone" expansion.

Given that most of the current studies of braided stents are based on straight vessels, it is a challenge and difficult work to evaluate the "Dogbone" of stents in the curved vessels. Therefore, the purpose of this paper is to investigate the mechanical properties of parameterized braided stents by balloon-expanding in the curved vessels. In this study, the contents are as follows: i) investigate the "Dogbone" behaviors of braided stents based on different parameters (strut diameter, braided angle, and the circumferential number of unit cell) in the curved vessels; ii) especially, improve the calculation method of "Dogbone" deformations for braided stents in the curved vessels; iii) analyze the fatigue properties of "Dogbone" stents; iv) analyze the influence of "Dogbone" stents on stress distribution of curved vascular walls.

## 2. Materials and methods

### *2.1. Modeling braided stents and curved vessels*

All braided-stent models considered in this study were built using the Kratos plugin of open-source software GiD 15.0.2 to build braided stents [27], as shown in Figure 2. On the basis of the previous research [2,3,5,28], given that the strut diameter, braiding angle, and the circumferential number of unit cell are the three main factors for designing stents, therefore, strut radius $t$ was 100, 125 and 150 μm, the braiding angle $\alpha$ was 30, 40, and 50°, and the circumferential number of unit cell $N$ = 8, $N$ = 10, and $N$ = 12 was considered, respectively. The design scheme of stents was listed

in Table 1. The inner radius $R$ of the braided stent was 5 mm, the length $L$ of the stent was 40 mm, respectively. Stainless steel (AISI 316L) material was modeled using an elastic-plastic constitutive material model for the braided stent. The material parameters in this study were obtained from previous research [29], as listed in Table 2.

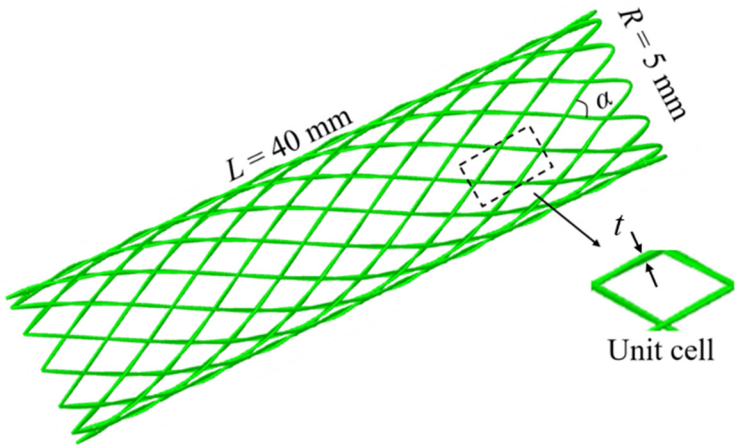


**Figure 2.** Braided stents.

**Table 1**. Optimal design scheme of braided stents.

| Specimen number | Strut diameter $t$ (μm) | Braiding angle $\alpha$ (°) | The circumferential number of unit cell $N$ |
|---|---|---|---|
| 1 | 100 | 30 | 8 |
| 2 | 125 | 30 | 8 |
| 3 | 150 | 30 | 8 |
| 4 | 100 | 40 | 8 |
| 5 | 125 | 40 | 8 |
| 6 | 150 | 40 | 8 |
| 7 | 100 | 50 | 8 |
| 8 | 125 | 50 | 8 |
| 9 | 150 | 50 | 8 |
| 10 | 100 | 30 | 10 |
| 11 | 125 | 30 | 10 |
| 12 | 150 | 30 | 10 |
| 13 | 100 | 40 | 10 |
| 14 | 125 | 40 | 10 |
| 15 | 150 | 40 | 10 |
| 16 | 100 | 50 | 10 |
| 17 | 125 | 50 | 10 |
| 18 | 150 | 50 | 10 |

*Continued on next page*

| Specimen number | Strut diameter $t$ (μm) | Braiding angle $\alpha$ (°) | The circumferential number of unit cell $N$ |
|---|---|---|---|
| 19 | 100 | 30 | 12 |
| 20 | 125 | 30 | 12 |
| 21 | 150 | 30 | 12 |
| 22 | 100 | 40 | 12 |
| 23 | 125 | 40 | 12 |
| 24 | 150 | 40 | 12 |
| 25 | 100 | 50 | 12 |
| 26 | 125 | 50 | 12 |
| 27 | 150 | 50 | 12 |

**Table 2.** Material parameters of the braided stents.

| Young's modulus (GPa) | Poisson's ratio | Ultimate tensile strength (MPa) | Yield strength (MPa) |
|---|---|---|---|
| 210 | 0.3 | 580 | 315 |

It was assumed that an ideal curved vessel was used to study the deformation after braided stent expanding in this paper. The curved vessel was a total length of 50 mm along the axial direction, an inner diameter of 4 mm, a wall thickness of 1 mm, and the bending angle of 60°. As Schiavone and Zhao [30] mentioned, the vessel wall was divided into three layers, namely intima (0.27 mm), media (0.35 mm), and adventitia (0.38 mm). The curvature of the vessel is $R_c$ = 50 mm (shown in Figure 3). Since studying vascular, the commonly used constitutive models including Neo-Hookean, Mooney-Rivlin, the Ogden model and the Holzapfel model are proposed. Experimental studies have shown that the mechanical properties of healthy vascular walls were completely different in the circumferential and axial directions because of the helical collagen fibers surrounding the matrix [30]. Holzapfel et al. studied and proposed the anisotropic constitutive model for healthy vessels [31]. But atherosclerotic plaque can affect the fiber distribution and orientation of the vascular wall, the current analysis of atherosclerotic vessels is based on the 3rd order and 1st order of the Ogden model for artery and plaque, respectively [32]. The constitutive model selection for a highly non-linear behavior of artery is considered to be the most debatable. In this study, the curved vessel was assumed to be incompressible, isotropic, and hyperelastic vascular vessels model calcified by atherosclerosis. Considering store energy functions of the Ogden constitutive model [33,34], the third-order Ogden hyper-elastic strain energy potential was used to capture the bulk arterial material behavior, which is described as:

$$\mathrm{W} = \sum_{i=1}^{3} \frac{2\mu_i}{\alpha_i^2}\left(\lambda_1^{\alpha^i} + \lambda_2^{\alpha^i} + \lambda_3^{\alpha^i} - 3\right) + \sum_{i=1}^{3} \frac{1}{D_i}(J-1)^{2i} \tag{1}$$

Where $\lambda_i$ ($i$ = 1, 2, 3) are the stretches in the three principal directions, and $\mu_i$ (MPa), $\alpha_i$, and $D_i$ were model parameters. In this model, $\mu_i$ and $\alpha_i$ are associated with the shear modulus which can be calculated using the equation. $D_i$ ($D_2 = D_3 = 0$) represents the compressibility. This constitutive equation can simulate the hyper-elastic deformation of blood vessels. Values of model parameters are

given in Table 3 for the three-layered blood vessel.

**Table 3.** Values of the Ogden model parameters for the three vessel wall layers [33,34].

| Material | $\rho$ (kg/mm$^3$) | $\mu_1$ | $\mu_2$ | $\mu_3$ | $\alpha_1$ | $\alpha_2$ | $\alpha_3$ | $D_1$ |
|---|---|---|---|---|---|---|---|---|
| Intima | 1.07E-6 | -7.04 | 4.23 | 2.85 | 24.48 | 25.00 | 23.54 | 8.95E-7 |
| Media | 1.07E-6 | -1.23 | 0.88 | 0.45 | 16.59 | 16.65 | 16.50 | 5.31E-6 |
| Adventitia | 1.07E-6 | -1.28 | 0.85 | 0.44 | 24.63 | 25.00 | 23.74 | 4.67E-6 |

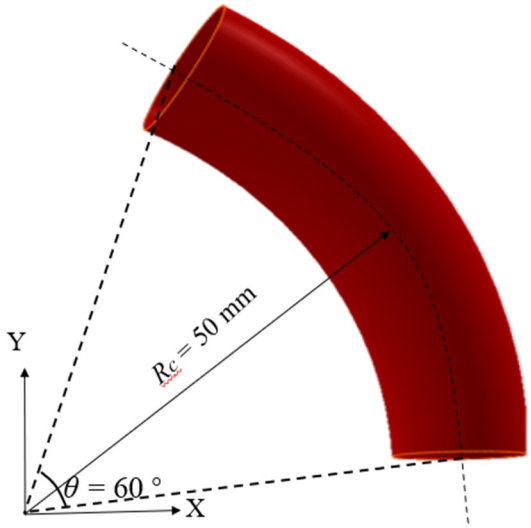


**Figure 3.** The model of curved vessel.

*2.2. Calculation method of "Dogbone" deformation in the curved vessels*

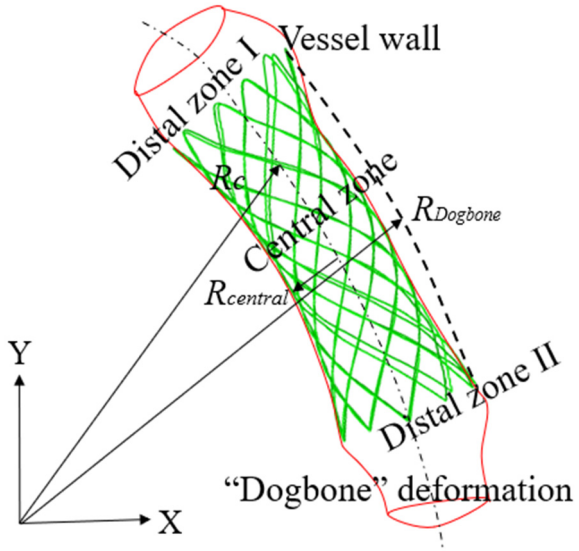


**Figure 4.** "Dogbone" deformation in the curved vessel.

For the calculation Eq (2) "Dogbone" of braided stents in a straight vessel does not fit into the curved vessel due to different deformation behaviors of stents, because the stent will not completely contact with the vascular wall due to different bending degrees, especially for the vessel with uneven bending, which causes the radius $R_{distal}$ of two distal zones of "Dogbone" stent will be unequal, i.e., $R_{distal\text{-}I} \neq R_{distal\text{-}II}$. But the radius $R_{distal}$ of two distal zones in the straight is equal value. Therefore, the improved formula of "Dogbone" was provided. Extracting the bus bar of the curved vessel was a key step, and it was the $R_c$ of the bus bar radius. When the stent generated the "Dogbone" deformation, the two distal zones of the stent in the plane with the bus bar of the vessel were connected and regarded as a new arc with a radius $R_{Dogbone}$, which avoided the case of unequal radius of two distal zones, as shown in Figure 4. Finally, the "Dogbone" formula in the curved vessel was given:

$$Dogbone = (R_{distal} - R_{central}) / R_{central} \tag{2}$$

$$Dogbone = (R_{Dogbone} - R_c) / R_c \tag{3}$$

For the Eq (3), if $R_{Dogbone} - R_c = R_{central}$, then stent with no "Dogbone" deformation. In the Eq (2), $R_{diatal}$ is the raduis of distal zones, and $R_{central}$ is the radius of central zone, as shown in Figure 1(b). In the Eq (3), $R_{Dogbon}$ is a new arc radius, $R_c$ is the bus bar radius, $R_{central}$ is the central radius after stent expanding.

### *2.3. Numerical simulation*

Numerical simulation has been widely used in analyzing stent deformation due to its accurate results and cost-saving [35−38]. The static analysis in this study was carried out by *Abaqus* 2016 solver (*Dassault Simulia Company*). The element of the braided stent was beam B31, the balloon element was surface SFM3D4, and the blood vessel element was C3D8RH. The contact between the outer surface of the balloon and the braided stent was set as point-surface contact. The contact between the inner surface of the vessel and the braided stent was also set as point-surface contact, the sliding formulation was finite sliding in *Abaqus* 2016. To prevent relative slip movement during the expansion, the penalty function was adopted for the tangential behavior of the vessel, stent, and balloon, the friction coefficient was set as 0.2. The 5.2 mm radial displacement load was applied on the inner surface of the balloon, and the stent expands under the action of the balloon. Based on these simulation conditions, the stent deformation in the curved vessels was mimicked.

## 3. Results

### *3.1. Influence of strut diameters on "Dogbone" deformations*

Based on the results of finite analysis, the "Dogbone" deformations of braided stents listed in Table A1 (Appendix) were calculated by the method proposed in Section 2.2. Using *Origin* 2017 data software (*Originlab Company*), the "Dogbone" deformation data were fitted and compared, as shown in Figure 5. Specimen numbers 1−3 stents, the "Dogbone" is 0.244 (specimen number 1 stent with 100 μm), 0.294 (specimen number 2 stent with 125 μm), and 0.323 (specimen number 3 stent with 150 μm), respectively. Similarly, according to Figure 5 and Table A1, the nine curves all showed the common rule, i.e., the larger the strut diameter, the more obvious the "Dogbone"

deformation. This regularity was very important for studying the effect of strut diameter on the mechanical behaviors of braided stents. The precondition of analyzing the influence of strut diameter on "Dogbone" deformations was that the braiding angle and the circumferential number of unit cell remained unchanged. For this phenomenon, it could be explained that in the process of stent expanding, the strut diameter affected the relative sliding between struts. Because the strut diameter increased the contact area between struts, which made the stent generate greater friction. When the stent expanded under the effect of the balloon, the greater friction prevented stent deformation. Therefore, when the stent expanded radially under the action of the balloon, the deformation between struts became smaller with the increase of diameter, and the warping occurred at both ends of the braided stent, resulting in the "Dogbone" deformations. On the contrary, struts with smaller diameter were easily prone to slide to each other when stents expanded because of weak friction between struts, which made stents less tend to generate "Dogbone" deformation.

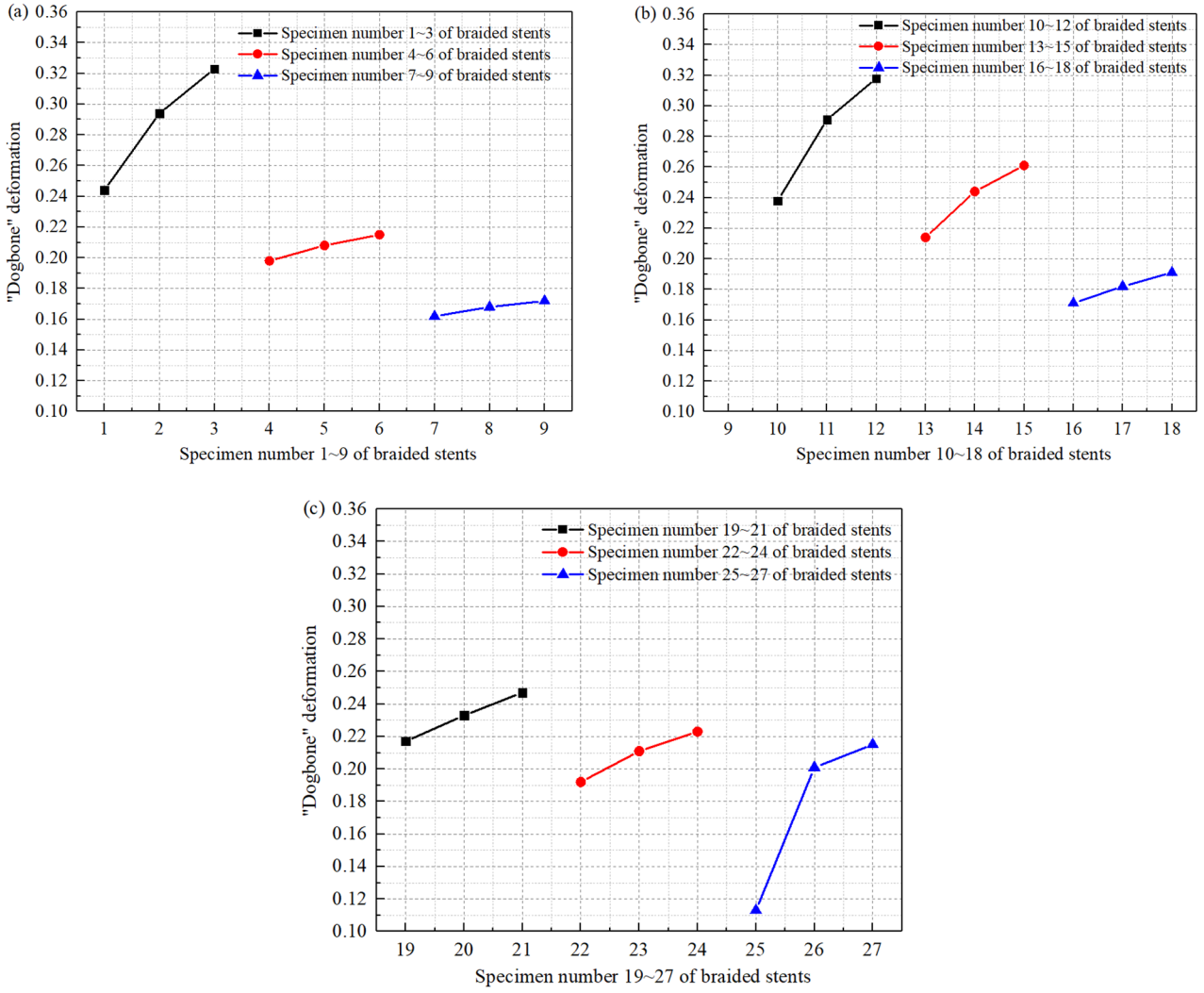


**Figure 5.** Influence of strut diameter on "Dogbone" deformations of braided stents: (a) specimen numbers 1−9; (b) specimen numbers 10−18; (c) specimen numbers 19−27.

### *3.2. Influence of braiding angles on "Dogbone" deformations*

By setting strut diameter and the circumferential number of unit cell were constant, the impact of braiding angle on "Dogbone" behaviors was shown in Figure 6. These curves showed obviously that the larger braiding angle improved the "Dogbone" deformation of stents. With the braiding angle increasing, the "Dogbone" deformation became smaller. This regularity also was very important for studying the effect of braiding angle on the "Dogbone" behaviors, which also verified that braiding angle was a key impact factor on the deformations of stents [2−4]. In the curved vessel of this study, the braiding angle still was the governing factor for the mechanics of braided stents. The results were explained that the braiding angle determined the number of axial unit cell of stents, the larger the braiding angle, and led to an intensive porosity of stent and a higher strut density, which contributed to improving the flexibility of braided stents. Besides, individual struts could rotate relative to one another during the radial expansion of stents. Inversely, for a smaller braiding angle, struts were less likely to slide or rotate past one another. Consequently, in the process of stent expanding and bending in the curved vessels, a larger braiding angle was conducive to deforming uniformly.

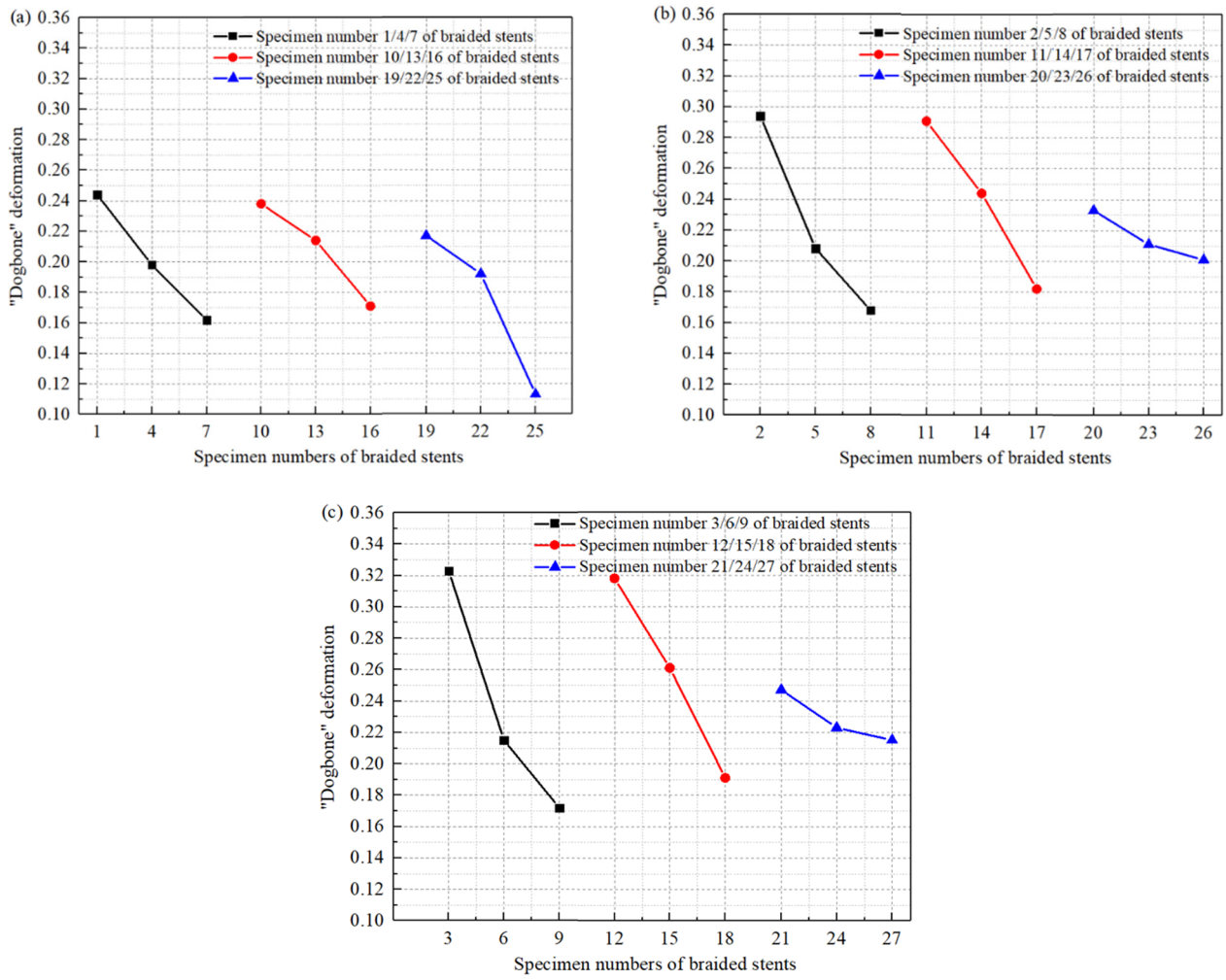


**Figure 6.** Influence of braiding angle on "Dogbone" deformations of braided stents: (a) specimen numbers 1/4/7; 10/13/16; 19/22/25; (b) specimen numbers 2/5/8; 11/14/17; 20/23/26; (c) specimen numbers 3/6/9; 12/15/18; 21/24/27.

### *3.3. Influence of the circumferential number of unit cell on "Dogbone" deformations*

Compared with strut diameter and braiding angle, there were different results that the influence of the circumferential number of unit cell on "Dogbone" deformations. From Figure 7(a), when the strut diameter and braiding angle were constant values, the "Dogbone" deformations were smaller with the circumferential number of unit cell increasing from 8 to 12. But in Figure 7(b), the "Dogbone" deformations were first bigger, and then smaller with the circumferential number of unit cell increasing from 8 to 12. Especially, there was no obvious regularity when braiding angle $\alpha = 50°$, although the circumferential number of unit cell increased from 8 to 12. Because the circumferential number of unit cell had little effect on the relative slip and friction between struts, it was difficult to change and affect the axial flexibility of stents. The finite element results showed that when the braiding angle $\alpha$ was 30 and 40° respectively, the "Dogbone" deformation of stents presented totally opposite trends. Because the circumferential number of unit cell did not affect the mutual sliding and axial porosity of stents, when braided stents expanded radially, both ends of stents would still warp, resulting in forming "Dogbone" deformation. Therefore, in terms of the circumferential number of unit cell, changing the circumferential number had little effect on the "Dogbone" deformation.

The influence of design parameters on "Dogbone" of braided stents was shown by numerical simulation. It could be concluded that the braiding angle and strut diameter had a greater influence on "Dogbone" deformation than the circumferential number of unit cell. When designing braided stents, three design factors including strut diameter, braiding angle, and the circumferential number of unit cell should be fully considered, and the influence of these design parameters on "Dogbone" deformation should be paid special attention. Especially, smaller strut diameter and larger braiding angle should be selected to effectively improve the flexibility of stents.

This is an important work to study "Dogbone" deformation of braided stents in the curved vessels. Although [11] also reported "Dogbone" deformation of stents in the curved vessels, they only evaluated existing commercial stents without optimization and improvement, and the degree of vascular bending simulated by them was small. In this study, not only do vessels with a high degree of curvature be simulated, but the stent structure is optimized. For eliminating the "Dogbone" deformation of stents in the straight vessels, Wang et al. [26] improved the geometry of a stent, they increased the strut width at end rings of stents in the circumferential directions. Although this method could minimize the "Dogbone" deformation, it required the length of balloon matching stents to achieve good results. Furthermore, De Beule et al. [24] studied and compared the influence of different expansion modeling strategies of the new generation balloon-expandable stent on "Dogbone" deformation, and did not design and optimize the structure of the stent. Comparing these existing studies on "Dogbone" of stents, this study analyzes the influence of strut diameter, braiding angle, and the circumferential number of unit cell on "Dogbone" deformation in the curved vessels by optimizing stents. Importantly, a more suitable method for calculating the "Dogbone" deformation in the curved vessels has been improved.

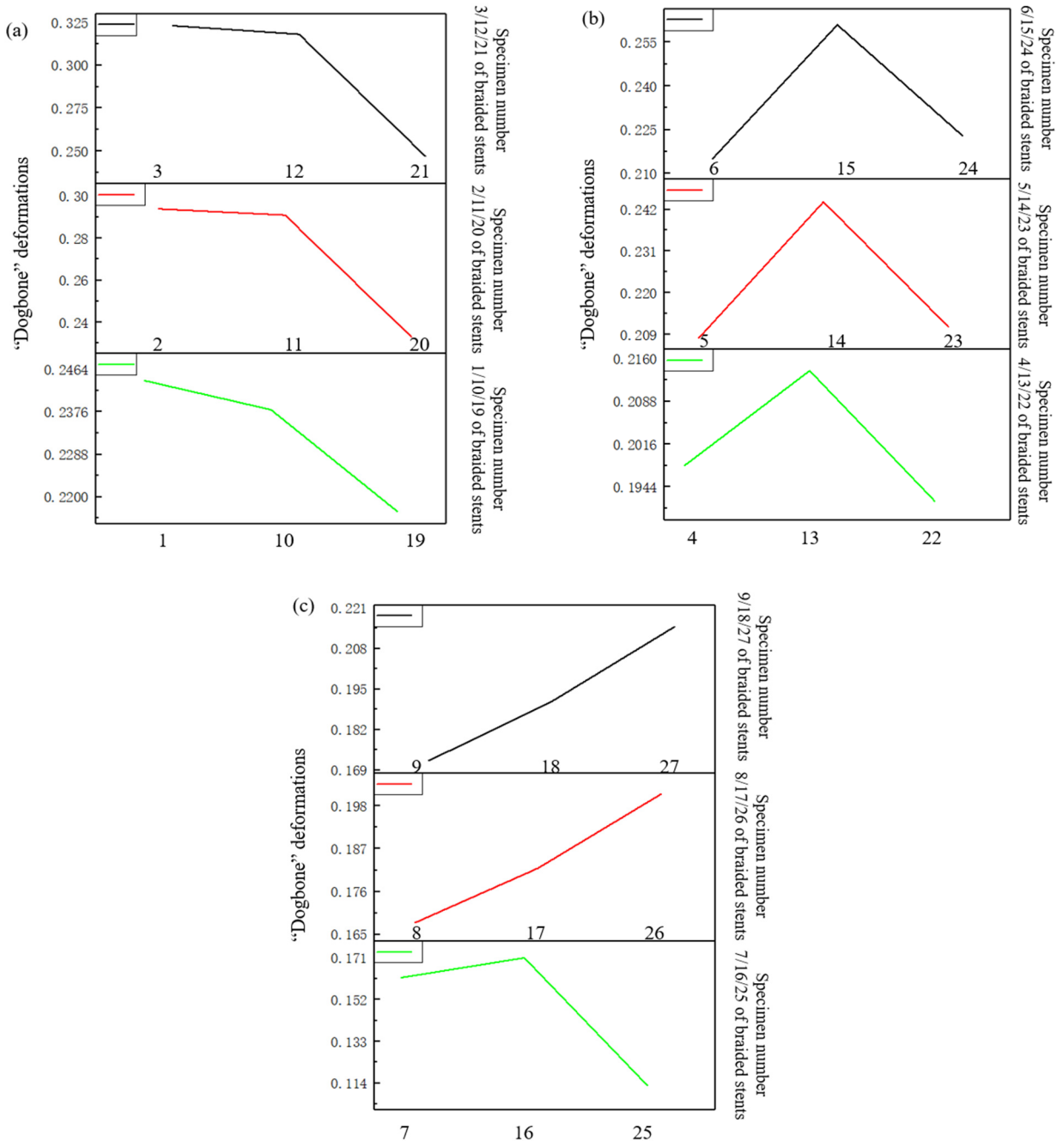


**Figure 7.** Influence of the circumferential number of unit cell on "Dogbone" deformations of braided stents: (a) specimen numbers 1/10/19; 2/11/20; 3/12/21; (b) specimen numbers 4/13/22; 5/14/23; 6/15/24; (c) specimen numbers 7/16/25; 8/17/26; 9/18/27.

## 4. Discussion and analysis fatigue of braided stents and damage of "Dogbone" deformation to curved vascular walls

### *4.1. Influence of "Dogbone" on fatigue properties*

The assessment of fatigue performance is the primary importance to assure the effectiveness of the stenting procedure [39]. The fatigue prediction is of great significance for designing stent

and clinical application. Stent fatigue is defined that the stress concentration and fracture under the action of long-term pulsating contact from the vessel wall, which results in losing the function of opening up the blood vessel [29,36,40−42]. The fatigue fracture risk of stents is assessed on the basis of amplitude stress and mean stress, the amplitude stress reflects the oscillations of the stent under the action of vascular pulsation [36], and the mean stress reflects the average deformation of stent undergoing multiple contacts from the vessel wall. For steps of the loading cycle, the maximum in absolute value between first and third principal stress is identified at each element and stored with the proper sign, thus obtaining the amplitude stress and the mean stress, respectively, the following relations are used:

$$\sigma_{amplitude} = \frac{\sigma_{max} - \sigma_{min}}{2} \tag{4}$$

$$\sigma_{mean} = \frac{\sigma_{max} + \sigma_{min}}{2} \tag{5}$$

In this section, a common way to evaluate the fatigue life of stents was to consider the amplitude stress and mean stress. Figure 8 showed the amplitude stress and mean stress of specimen numbers 1−9 braided stents with "Dogbone" (the rest of specimen numbers 10−27 braided stents as shown in Figures A1 and A2 of Appendix), all amplitude stress and mean stress were listed in the Table 4. To analyze the fatigue properties of "Dogbone" stents, all 27 braided stents were divided into 9 groups, i.e., specimen numbers 1−3, 4−6, 7−9, 10−12, 13−15, 16−18, 19−21, 22−24, 25−27. As can be concluded from Table 4, the fatigue resistance of stents decreased with the increase of the "Dogbone" deformation. For example, the maximum amplitude stress 113.7 MPa and the maximum mean stress 308.4 MPa of specimen number 3 stent with larger "Dogbone" 0.323 were greater than specimen number 2 stent with 0.294 "Dogbone" (the max. amplitude stress 939.2 MPa and the maximum mean stress 268.9 MPa) and specimen number 1 stent with 0.244 "Dogbone" (the maximum amplitude stress 73.49 MPa and the maximum mean stress 231.1 MPa). The conclusion that larger "Dogbone" deformations of stents, the more prone to fatigue failure occurred, was also applicable to the other 8 groups. These results confirmed that the larger the "Dogbone" deformation, the worse the fatigue resistance of stents [43]. Among the 9 groups of stents, only the strut diameter was a variable, and the other two design parameters were constant. Specimen numbers 1−3 braided stents were still used as examples to explain. The strut diameter increased from 100 to 150 μm, as discussed in Section 3.1, the increase of strut diameter made the friction worse and inhibited the relative sliding of the struts. Due to the larger diameter of the strut, when the stent was subjected to the diastolic and systolic action of pulsation in the curved vessels, the friction between struts hindered the relative movement of struts. The stent could not relieve the pressure effect from the vascular wall by sliding struts, which led to changing the stress concentration and distribution of the stent. [3,6,44,45]. On the contrary, the smaller strut diameter could ease the pulsation effect of vascular vessels by relative slipping.

Especially, braiding angle also had an impact on fatigue performance. For instance, among specimen numbers 1 and 4 and 7 stents, the specimen number 7 stent (braiding angle = 50°) with smallest "Dogbone" deformation 0.162, but it was the maximum amplitude stress 172.9 MPa and the maximum mean stress 613.8 MPa were higher than other two stents (specimen number 1 stent (braiding angle = 30°) with 0.244 "Dogbone", the maximum amplitude stress 734.9 MPa and the maximum mean stress 231.1 MPa; specimen number 4 stent (braiding angle = 40°) with 0.198

"Dogbone", the maximum amplitude stress 154.0 MPa and the maximum mean stress 377.5 MPa, respectively). Similarly, specimen numbers 2/5/8, 3/6/9 (in Figure 8), specimen numbers 10/13/16, 11/14/17, 12/15/18 (in Figure A1), specimen numbers 19/22/25, 20/23/26, 21/24/27 (in Figure A2), all showed that the fatigue performance was directly related to braiding angle. The results were explained that the braiding angle densified the struts density, the contact area between the stent and the inner wall of the vessel increased after the stent expanded. Under the effect of vascular pulsation, more struts were involved in the interaction between the stents and the vascular vessels, which made the stents more prone to fatigue.

The circumferential number of unit cell as another design variable had little effect on the fatigue of stents. Through comprehensive comparison of specimen numbers 1/10/19, 2/11/20, 3/12/21, 4/13/22, 5/14/23, 6/15/24, 7/16/25, 8/17/26, 9/18/27 (in Figures 8, A1, and A2), it could be found that when the other two design parameters were constant, the amplitude stress and mean stress of stents generated relatively smaller changes though the circumferential number of unit cell increased. Because the change of the circumferential number of unit cell had no influence on the friction between the struts and had little influence on the density of the stents, the stress change under the action of the vascular wall was small and the fatigue damage was not obvious.

In conclusion, the "Dogbone" deformation of stents in the curved vessels has a great influence on the fatigue performance, and these influencing factors are mainly the strut diameter and the braiding angle. Therefore, reasonable parameters can be designed to reduce the "Dogbone" deformation and fatigue damage.

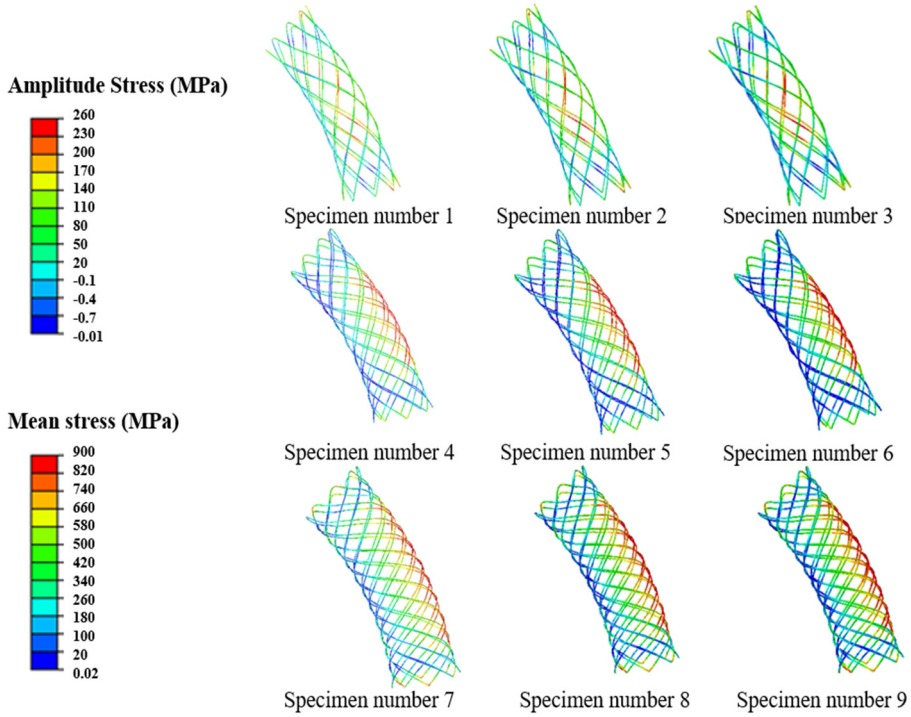


**Figure 8**. Fatigue diagram for fully radial expansion of the braided stent in the curved vessel: the amplitude stress and mean stress of specimen numbers 1−9 stents.

**Table 4.** The maximum amplitude stress and mean stress of all stents.

| Specimen number | the maximum amplitude stress (MPa) | the maximum mean stress (MPa) | Specimen number | the maximum amplitude stress (MPa) | the maximum mean stress (MPa) |
|---|---|---|---|---|---|
| 1 | 73.49 | 231.1 | 15 | 234.4 | 529.3 |
| 2 | 93.92 | 269.8 | 16 | 163.4 | 623.4 |
| 3 | 113.70 | 308.4 | 17 | 200.9 | 747.0 |
| 4 | 154.0 | 377.5 | 18 | 238.5 | 881.6 |
| 5 | 196.0 | 453.4 | 19 | 156.8 | 263.1 |
| 6 | 238.0 | 529.5 | 20 | 206.4 | 330.0 |
| 7 | 172.9 | 613.8 | 21 | 251.9 | 400.3 |
| 8 | 220.3 | 756.0 | 22 | 156.5 | 379.5 |
| 9 | 251.7 | 851.3 | 23 | 197.5 | 454.4 |
| 10 | 156.1 | 259.7 | 24 | 238.0 | 529.4 |
| 11 | 211.1 | 342.8 | 25 | 166.2 | 644.0 |
| 12 | 262.2 | 420.5 | 26 | 204.9 | 774.8 |
| 13 | 153.9 | 378.5 | 27 | 242.6 | 894.7 |
| 14 | 194.1 | 452.9 | | | |

*4.2. The influence of "Dogbone" deformation on the stress distribution of curved vascular walls*

Investigating the stresses of curved vessels is important, because stent implantation in the vascular lumen can cause stress concentration of the vascular walls. Therefore, the effects of different "Dogbone" stents on the vascular wall were mimicked by finite element simulation. The stress distribution in the curved vessels was shown in Figures 9 and A3. For clear analysis and comparison, the maximum Von Mises stresses of all vessel walls were listed in Table 5. By studying the stress distribution in all the vessel walls, it was found that the stress distribution on the curved vessel wall was very uniform except where it was in contact with the "Dogbone" deformation of the stent. The "Dogbone" deformations of stents generated a huge impact on the stress of curved vascular walls. For example, among specimen numbers 1−3, the maximum Von Mises stress of vascular vessel was 0.09828 MPa under specimen number 1 stent with 0.244 "Dogbone" deformation, the maximum Von Mises stress of vascular vessel was 0.1922 MPa under specimen number 2 stent with 0.294 "Dogbone" deformation, but the maximum Von Mises stress of vascular vessel was 0.5479 MPa under specimen number 1 stent with 0.323 "Dogbone" deformation. The stress distribution of specimen numbers 10−27 stents vascular walls also showed the same trends in Figure A3. It could be concluded that the "Dogbone" stents in the curved vessels led to vascular stress concentration. Because both ends of the "Dogbone" stents expanded more than other parts, and presented an upturned state, one end of the strut directly contacted the inner wall of the vessel, which resulted in damage to the thin vascular walls. Among the braided stents with "Dogbone" deformations, the specimen number 25 stent with strut diameter $t$ = 100 μm, braiding angle = 50° and the circumferential number of unit cell $N$ = 12 generated the smallest "Dogbone" = 0.113 (in Table A1), which made the curved vessels generate the minimum Mises stress 0.04009 MPa. Therefore, in terms of the damage of "Dogbone" deformations to

vascular vessels, the parameters of braided stents should be set strut diameter $t$ = 100 μm, braiding angle = 50°, and the circumferential number of unit cell $N$ = 12.

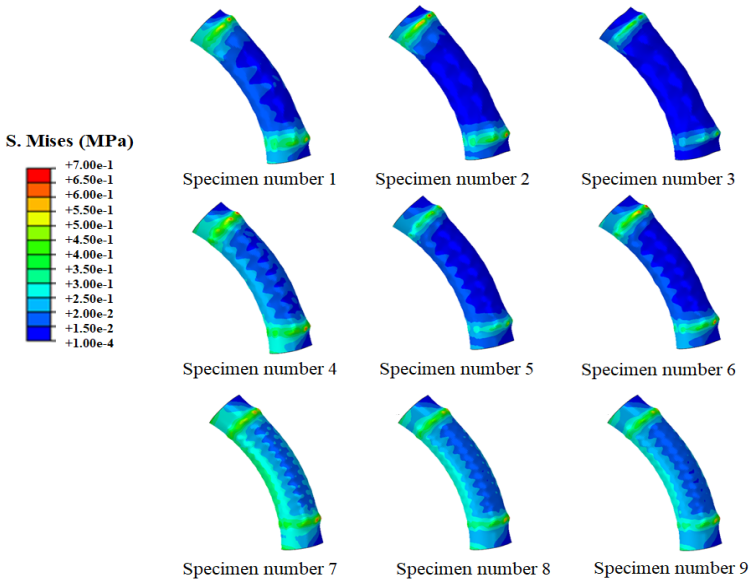


**Figure 9.** Stress distribution of curved vessel walls from the specimen number 1 stents with "Dogbone" deformation.

**Table 5.** Stress distributions of all vessel walls.

| Specimen number | the maximum Von Mises stress (MPa) | Specimen number | the maximum Von Mises stress (MPa) | Specimen number | the maximum Von Mises stress (MPa) |
|---|---|---|---|---|---|
| 1 | 0.09828 | 10 | 0.10420 | 19 | 0.11920 |
| 2 | 0.19220 | 11 | 0.31230 | 20 | 0.26420 |
| 3 | 0.54790 | 12 | 0.54610 | 21 | 0.61300 |
| 4 | 0.05725 | 13 | 0.05770 | 22 | 0.06691 |
| 5 | 0.12090 | 14 | 0.09528 | 23 | 0.09900 |
| 6 | 0.12010 | 15 | 0.13570 | 24 | 0.13790 |
| 7 | 0.03555 | 16 | 0.03688 | 25 | 0.04009 |
| 8 | 0.04267 | 17 | 0.04437 | 26 | 0.04660 |
| 9 | 0.04457 | 18 | 0.04666 | 27 | 0.04901 |

## 5. Conclusions

In this study, the "Dogbone" of braided stents with different parameters including strut diameter, braiding angle, and the circumferential number of unit cell are evaluated and investigated in the curved vessels. Besides, because "Dogbone" deformation in the curved vessel is different from that in the straight vessel, the equation to calculate the "Dogbone" is improved. The numerical results showed that the larger strut diameter could cause more serious "Dogbone" deformations. The larger

braiding angle could improve the "Dogbone" deformations of stents. The effect of the circumferential number of unit cell on "Dogbone" deformation was less than that of strut diameter and braiding angle. In addition, the fatigue performance of braided stents and the stress distributions of curved vascular walls caused by "Dogbone" deformations were also analyzed. Stents are implanted to stay in the body for a long time to support blocked blood vessels. Therefore, clinical applications should be considered comprehensively and evaluated when designing braided stents. "Dogbone" deformation not only results in great stress and fatigue fracture of stents, but also causes the stress concentration of the vascular walls, and finally triggers intimal hyperplasia and ISR.

There are still some limitations in this paper, some factors affecting stent properties and behaviors in the curved vessels, such as hemodynamics, have not been fully considered. In future studies, the premise of stent design should be patient-specific, and pathological vessels should be taken as the target deformation of the stent, to ensure that the stent can maintain the same shape as the vessel and have good mechanical properties.

## Acknowledgments

The authors would like to thank the School of Mechanical Engineering of Beijing Institute of Technology (BIT), and Institute of Engineering Medicine of Beijing Institute of Technology (BIT). We are especially grateful to the team including Giuliodori, A., Hernández, J., and Soudah, E. for their support of our GiD open source software.

## Conflict of interest

The authors declare no conflict of interests.

## References

1. R. W. Günther, D. Vorwerk, K. Bohndorf, K. C. Klose, D. Kistler, H. Mann, et al., Venous stenoses in dialysis shunts: Treatment with self-expanding metallic stents, *Radiology*, **170** (1989), 401−405. https://doi.org/10.1148/radiology.170.2.2521397
2. C. G. Mckenna, T. J. Vaughan, An experimental evaluation of the mechanics of bare and polymer-covered self-expanding wire braided stents, *J. Mech. Behav. Biomed. Mater.*, **103** (2020), 103549. https://doi.org/10.1016/j.jmbbm.2019.103549
3. C. G. Mckenna, T. J. Vaughan. A finite element investigation on design parameters of bare and polymer-covered self-expanding wire braided stents, *J. Mech. Behav. Biomed. Mater.*, **115** (2021), 104305. https://doi.org/10.1016/j.jmbbm.2020.104305
4. K. C. Ueng, S. P. Wen, C. W. Lou, J. H. Lin. Stainless steel/nitinol braid coronary stents: Braiding structure stability and cut section treatment evaluation, *J. Ind. Text.*, **45** (2016), 965−977. https://doi.org/10.1177/1528083714550054
5. Q. Zheng, H. Mozafari, Z. Li, L. Gu, M. An, X. Han, et al., Mechanical characterization of braided self-expanding stents: Impact of design parameters, *J. Mech. Med. Biol.*, **19** (2019), 1950038. https://doi.org/10.1142/S0219519419500386

6. F. Zhao, W. Xue, F. Wang, J. Sun, J. Lin, L. Liu, et al., Braided bioresorbable cardiovascular stents mechanically reinforced by axial runners, *J. Mech. Behav. Biomed. Mater.*, **89** (2019), 19−32. https://doi.org/10.1016/j.jmbbm.2018.09.003
7. J. Sun, K. Sun, K. Bai, S. Chen, F. J. Wang, F. Zhao, et al., A novel braided biodegradable stent for use in congenital heart disease: Short-term results in porcine iliac artery, *J. Biomed. Mater. Res. A*, **107** (2019), 1667−1677. https://doi.org/10.1002/jbm.a.36682
8. C. Shanahan, P. Tiernan, S. A. M. Tofail, Looped ends versus open ends braided stent: A comparison of the mechanical behaviour using analytical and numerical methods, *J. Mech. Behav. Biomed. Mater.*, **75** (2017), 581−591. https://doi.org/10.1016/j.jmbbm.2017.08.025
9. H. Zahedmanesh, D. John Kelly, C. Lally, Simulation of a balloon expandable stent in a realistic coronary artery-determination of the optimum modelling strategy, *J. Biomech.*, **43** (2010), 2126−2132. https://doi.org/10.1016/j.jbiomech.2010.03.050
10. L. Wei, Q. Chen, Z. Li, Study on the impact of straight stents on arteries with different curvatures, *J. Mech. Med. Biol.*, **16** (2016), 1−13. https://doi.org/10.1142/S0219519416500937
11. L. Wei, H. L. Leo, Q. Chen, Z. Li, Structural and hemodynamic analyses of different stent structures in curved and stenotic coronary artery, *Front Bioeng. Biotechnol.*, **7** (2019), 1−13. https://doi.org/10.3389/fbioe.2019.00366
12. W. Wu, W. Q. Wang, D. Z. Yang, M. Qi, Stent expansion in curved vessel and their in teractions: A finite element analysis, *J. Biomech.*, **40** (2007), 2580−2585. https://doi.org/10.1016/j.jbiomech.2006.11.009
13. S. Kasiri, D. J. Kelly, An argument for the use of multiple segment stents in curved arteries, *J. Biomech. Eng.*, **133** (2011), 2−6. https://doi.org/10.1115/1.4004863
14. Y. Han, W. Lu, Optimizing the deformation behavior of stent with nonuniform Poisson's ratio distribution for curved artery, *J. Mech. Behav. Biomed. Mater.*, **88** (2018), 442−452. https://doi.org/10.1016/j.jmbbm.2018.09.005
15. J. A. Ormiston, S. R. Dixon, M. W. I. Webster, P. N. Ruygrok, J. T. Stewart, I. Minchington, et al., Stent longitudinal flexibility: A comparison of 13 stent designs before and after balloon expansion, *Catheter Cardiovasc. Interv.*, **50** (2000), 120−124. https://doi.org/10.1002/(SICI)1522-726X(200005)50:1<120::AID-CCD26>3.0.CO;2-T
16. B. P. Murphy, P. Savage, P. E. McHugh, D. F. Quinn, The stress-strain behavior of coronary stent struts is size dependent, *Ann. Biomed. Eng.*, **31** (2003), 686−691. https://doi.org/10.1114/1.1569268
17. R. Rieu, P. Barragan, V. Garitey, P. O. Roquebert, J. Fuseri, P. Commeau, et al., Assessment of the trackability, flexibility, and conformability of coronary stents: A comparative analysis, *Catheter Cardiovasc. Interv.*, **59** (2003), 496−503. https://doi.org/10.1002/ccd.10583
18. K. Mori, T. Saito, Effects of stent structure on stent flexibility measurements, *Ann. Biomed. Eng.*, **33** (2005), 733−742. https://doi.org/10.1007/s10439-005-2807-6
19. S. Pant, G. Limbert, N. P. Curzen, N. W. Bressloff, Multiobjective design optimisation of coronary stents, *Biomaterials*, **32** (2011), 7755−7773. https://doi.org/10.1016/j.biomaterials.2011.07.059
20. S. Tammareddi, G. Sun, Q. Li, Multiobjective robust optimization of coronary stents, *Mater. Des.*, **90** (2016), 682−692. https://doi.org/10.1016/j.matdes.2015.10.153

21. J. Raamachandran, K. Jayavenkateshwaran, Modeling of stents exhibiting negative Poisson's ratio effect, *Comput. Methods Biomech. Biomed. Eng.*, **10** (2007), 245−255. https://doi.org/10.1080/10255840701198004
22. P. K. M. Prithipaul, M. Kokkolaras, D. Pasini, Assessment of structural and hemodynamic performance of vascular stents modelled as periodic lattices, *Med. Eng. Phys.*, **57** (2018), 11−18. https://doi.org/10.1016/j.medengphy.2018.04.017
23. K. Maleckis, P. Deegan, W. Poulson, C. Sievers, A. Desyatova, J. MacTaggart, et al., Comparison of femoropopliteal artery stents under axial and radial compression, axial tension, bending, and torsion deformations, *J. Mech. Behav. Biomed. Mater.*, **75** (2017), 160−168. https://doi.org/10.1016/j.jmbbm.2017.07.017
24. M. De Beule, P. Mortier, S. G. Carlier, B. Verhegghe, R. Van Impe, P. Verdonck, Realistic finite element-based stent design: The impact of balloon folding, *J. Biomech.*, **41** (2008), 383−389. https://doi.org/10.1016/j.jbiomech.2007.08.014
25. G. R. Douglas, S. A. Phani, J. Gagnon, Analyses and design of expansion mechanisms of balloon expandable vascular stents, *J. Biomech.*, **47** (2014), 1438−1446. https://doi.org/10.1016/j.jbiomech.2014.01.039
26. W. Q. Wang, D. K. Liang, D. Z. Yang, M. Qi, Analysis of the transient expansion behavior and design optimization of coronary stents by finite element method, *J. Biomech.*, **39** (2006), 21−32. https://doi.org/10.1016/j.jbiomech.2004.11.003
27. A. Giuliodori, J. A. Hernández, D. Fernandez-Sanchez, I. Galve, E. Soudah, Numerical modeling of bare and polymer-covered braided stents using torsional and tensile springs connectors, *J. Biomech.*, **123** (2021), 110459. https://doi.org/10.1016/j.jbiomech.2021.110459
28. Z. Liu, L. Wu, J. Yang, F. Cui, G. Chen, Thoracic aorta stent grafts design in terms of biomechanical investigations into flexibility, *Math. Biosci. Eng.*, **18** (2020), 800−816. https://doi.org/10.3934/mbe.2021042
29. M. Azaouzi, A. Makradi, S. Belouettar, Numerical investigations of the structural behavior of a balloon expandable stent design using finite element method, *Comput. Mater. Sci.*, **72** (2013), 54−61. https://doi.org/doi:10.1016/j.commatsci.2013.01.031
30. Z. Y. Zhang, An experimental and theoretical study on the anisotropy of elastin network, *Ann. Biomed. Eng.*, **37** (2009), 1572−1583. https://doi.org/10.1007/s10439-009-9724-z
31. G. A. Holzapfel, G. Sommer, C. T. Gasser, P. Regitnig, Determination of layer-specific mechanical properties of human coronary arteries with nonatherosclerotic intimal thickening and related constitutive modeling, *Am. J. Physiol. Heart Circ. Physiol.*, **289** (2005), H2048. https://doi.org/10.1152/ajpheart.00934.2004
32. M. Umer, M. N. Ali, A. Mubashar, M. Mir, Computational modeling of balloon-expandable stent deployment in coronary artery using the finite element method, *Res. Rep. Clin. Cardiol.*, **10** (2019), 43−56. https://doi.org/10.2147/rrcc.s173086
33. A. Schiavone, L. G. Zhao, A study of balloon type, system constraint and artery constitutive model used in finite element simulation of stent deployment, *Mech. Adv. Mater. Mod. Process*, **1** (2015), 1−15. https://doi.org/10.1186/s40759-014-0002-x
34. H. Zahedmanesh, C. Lally, Determination of the influence of stent strut thickness using the finite element method: Implications for vascular injury and in-stent restenosis, *Med. Biol. Eng. Comput.*, **47** (2009), 385−393. https://doi.org/10.1007/s11517-009-0432-5

35. F. Migliavacca, L. Petrini, M. Colombo, F. Auricchio, R. Pietrabissa, Mechanical behavior of coronary stents investigated through the finite element method, *J. Biomech.*, **35** (2002), 803−811. https://doi.org/10.1016/S0021-9290(02)00033-7
36. M. Azaouzi, A. Makradi, S. Belouettar, Deployment of a self-expanding stent inside an artery: A finite element analysis, *Mater. Des.*, **41** (2012), 410−420. https://doi.org/10.1016/j.matdes.2012.05.019
37. L. Lei, X. Qi, S. Li, Y. Yang, Y. Hu, B. Li, et al., Finite element analysis for fatigue behaviour of a self-expanding Nitinol peripheral stent under physiological biomechanical conditions, *Comput. Biol. Med.*, **104** (2019), 205−214. https://doi.org/10.1016/j.compbiomed.2018.11.019
38. G. Praveen Kumar, A. Louis Commillus, F. Cui, A finite element simulation method to evaluate the crimpability of curved stents, *Med. Eng. Phys.*, **74** (2019), 162−165. https://doi.org/10.1016/j.medengphy.2019.07.017
39. L. Petrini, W. Wu, E. Dordoni, A. Meoli, F. Migliavacca, G. Pennati, Fatigue behavior characterization of nitinol for peripheral stents, *Funct. Mater. Lett.*, **5** (2012), 1250012. https://doi.org/10.1142/S1793604712500129
40. A. Meoli, E. Dordoni, L. Petrini, F. Migliavacca, G. Dubini, G. Pennati, Computational modelling of in vitro set-ups for peripheral self-expanding nitinol stents: the importance of stent-wall interaction in the assessment of the fatigue resistance, *Cardiovasc. Eng. Technol.*, **4** (2013), 474−484. https://doi.org/10.1007/s13239-013-0164-4
41. A. Meoli, E. Dordoni, L. Petrini, F. Migliavacca, G. Dubini, G. Pennati, Computational study of axial fatigue for peripheral nitinol stents, *J. Mater. Eng. Perform.*, **23** (2014), 2606−2613. https://doi.org/10.1007/s11665-014-0965-0
42. S. Gopal, S. Kim, R. Swift, B. Choules, Fatigue life estimation of nitinol medical devices, *Strain*, (2008), 1−10.
43. D. Elena, P. Lorenza, W. Wei, M. Francesco, D. Gabriele, P. Giancarlo, Computational modeling to predict fatigue behavior of NiTi stents: What do we need? *J. Funct. Biomater.*, **6** (2015), 299−317. https://doi.org/10.3390/jfb6020299
44. C. Shanahan, S. Tofail, P. Tiernan, Viscoelastic braided stent: finite element analysis and validation of crimping behaviour, *Mater. Design*, **121** (2017), 143−153. https://doi.org/10.1016/j.matdes.2017.02.044
45. J. H. Kim, T. J. Kang, W. R. Yu, Simulation of mechanical behavior of temperature-responsive braided stents made of shape memory polyurethanes, *J. Biomech.*, **43** (2010), 632−643. https://doi.org/10.1016/j.jbiomech.2009.10.032

## Appendix

**Table A1.** "Dogbone" deformations of braided stents.

| Specimen number | "Dogbone" | Specimen number | "Dogbone" | Specimen number | "Dogbone" |
|---|---|---|---|---|---|
| 1 | 0.244 | 10 | 0.238 | 19 | 0.217 |
| 2 | 0.294 | 11 | 0.291 | 20 | 0.233 |
| 3 | 0.323 | 12 | 0.318 | 21 | 0.247 |

*Continued on next page*

| Specimen number | "Dogbone" | Specimen number | "Dogbone" | Specimen number | "Dogbone" |
|---|---|---|---|---|---|
| 4 | 0.198 | 13 | 0.214 | 22 | 0.192 |
| 5 | 0.208 | 14 | 0.244 | 23 | 0.211 |
| 6 | 0.215 | 15 | 0.261 | 24 | 0.223 |
| 7 | 0.162 | 16 | 0.171 | 25 | 0.113 |
| 8 | 0.168 | 17 | 0.182 | 26 | 0.201 |
| 9 | 0.172 | 18 | 0.191 | 27 | 0.215 |

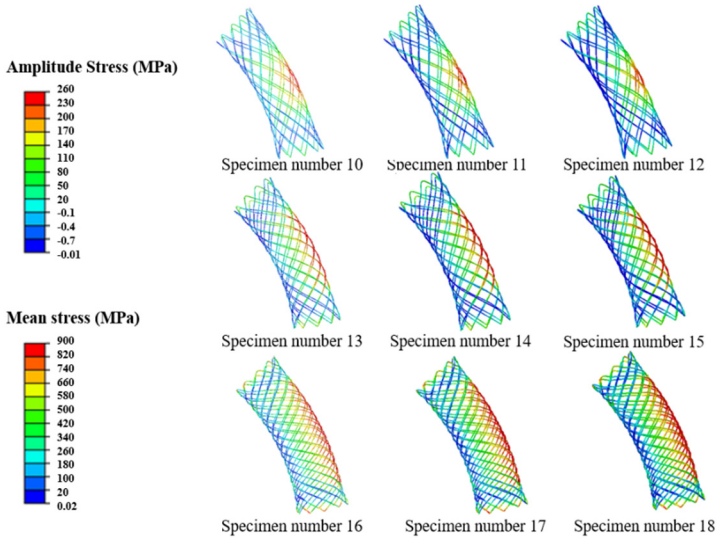


**Figure A1.** The amplitude stress and mean stress of specimen numbers 10−18 of braided stents. From the Figure A1, the strut diameters and braiding angles of specimens 10−18 stents have similar influence on the fatigue with specimens 1−9 in Figure 7.

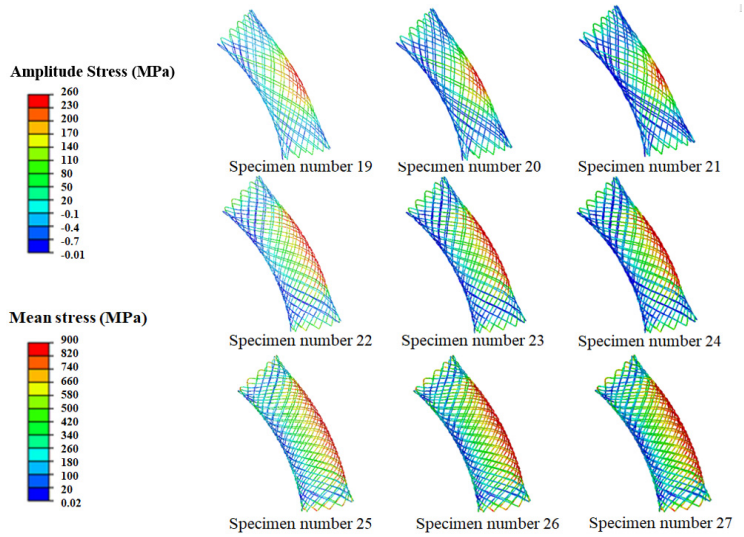


**Figure A2.** The amplitude stress and mean stress of specimen numbers 19−27 of braided stents. From the Figure A2, the strut diameters and braiding angles of specimens 19−27 stents have similar influence on the fatigue with specimens 1−9 in Figure 7.

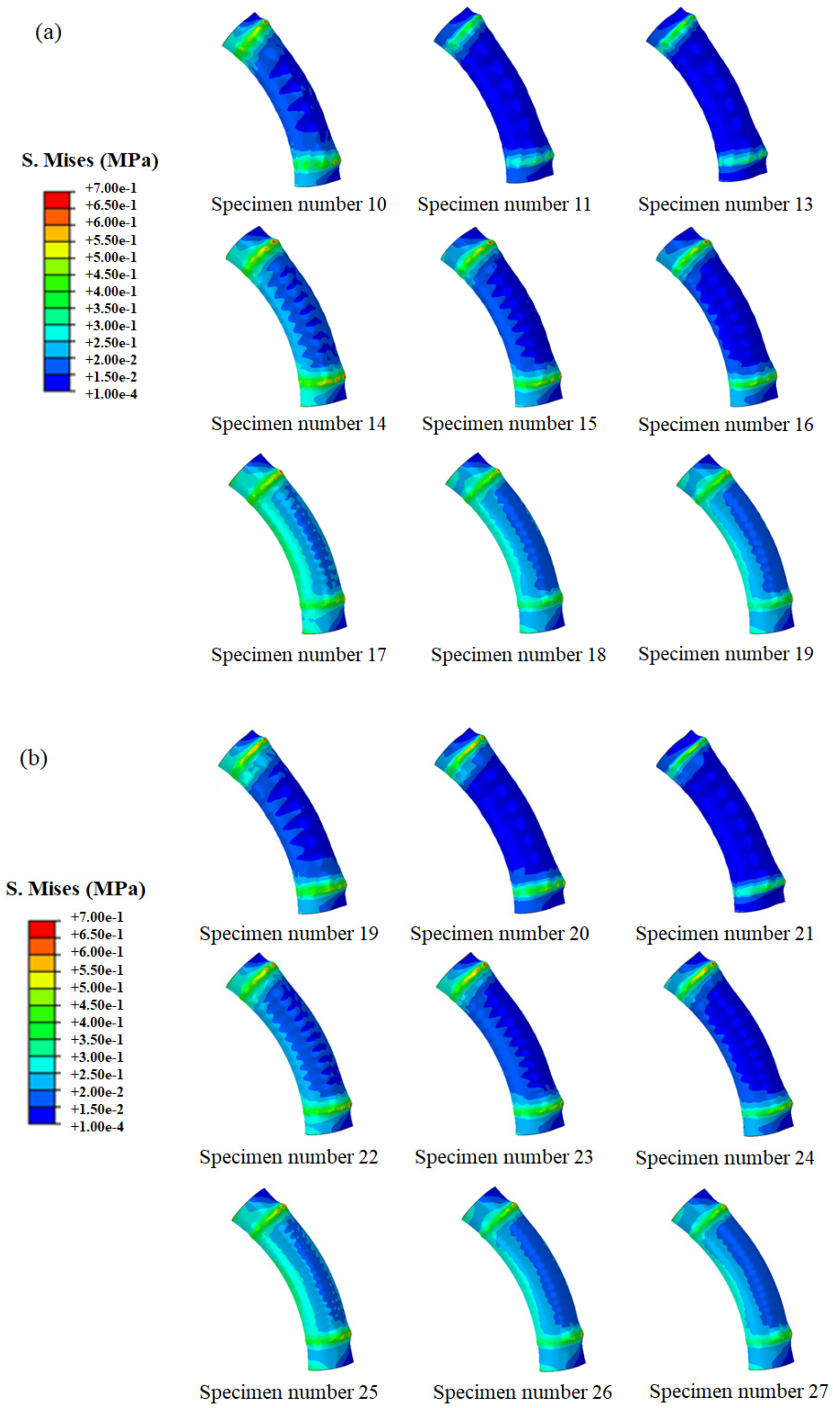


**Figure A3.** Stress distributions of all curved vessel walls: (a) and (b) showed the influence of "Dogbone" on the stress distributions of vascular vessels, i.e., the larger of "Dogbone" stent, the more serious stress concentration of the vascular vessels.

AIMS Press

©2022 the Author(s), licensee AIMS Press. This is an open access article distributed under the terms of the Creative Commons Attribution License (http://creativecommons.org/licenses/by/4.0)